Microwave Engineering
Ulm University

universität
ulm

A Modulation-Based Radar Target Simulator and Its Hardware Nonidealities

Pirmin Schoeder, Arne Martin, Benedikt Meinecke, David Werbunat, and Christian Waldschmidt

European Microwave Week 2022 Conference Proceedings. ©EuMA 2022.
Materials contained in the European Microwave Week 2022.
DOI: 10.23919/EuRAD54643.2022.9924830
ISBN: 978-2-8748-7071-2

A Modulation-Based Radar Target Simulator and Its Hardware Nonidealities

Pirmin Schoeder, Arne Martin, Benedikt Meinecke, David Werbunat, Christian Waldschmidt
Institute of Microwave Engineering, Ulm University, Germany
{name.surname}@uni-ulm.de

***Abstract* — Increasing demands in radar sensor performance for automotive applications require reliable test solutions for the development and verification. In this paper, a modulation-based radar target simulator suitable for automotive settings is presented. A cost-effective circuit with low complexity is proposed that modulates the radar signal directly in the E-Band without an intermediate frequency stage. Models are derived for predicting the limitations of such radar target simulators due to hardware nonidealities. The introduced radar target simulator is analyzed with respect to the derived nonidealities in order to predict its performance based on the models. As a verification, radar measurements with the target simulator are conducted, and compared with the models' predictions.**

***Keywords* — automotive radar, chirp-sequence modulation, FMCW radar, radar target simulator, system modelling.**

I. Introduction

The future of fully autonomous road traffic makes it necessary to have a high confidence in automotive radar sensors. This includes the correct estimation of crucial target attributes, like speed and location as well as the correct interpretation of whole traffic scenarios with a wide variety of objects and road users. To verify the functionality of whole radar systems, from sensor up to the signal processing, typical traffic scenarios simulated by a radar target simulator (RTS) can be used. By delaying and modulating the radar transmit signal, target responses with range and velocity can be simulated. But the realization of a time delay is costly, as it requires transmission lines for an increased time of flight [1], [2] or high speed data converters for digital realizations [3], [4]. In contrast, modulation-based RTSs can simulate targets with range and velocity for chirp-sequence frequency modulated (CS-FMCW) radars [5], which are predominantly used in automotive applications [6], [7], without a time delay. A modulation-based RTS enables the simulation of ranges from $0\,\mathrm{m}$ to the maximum range of the radar system. The fully analog implementation allows for low costs and the simulation of scenarios with a high target count [5], [8]. In this paper, the hardware of a novel modulation-based RTS is presented that modulates the transmit signal directly without an intermediate frequency (IF) stage. Compared to a design with an IF stage, the lowered circuit complexity of the new system reduces the costs of the RTS further. After the introduction of the RTS, the hardware nonidealities specific to the architecture are derived and investigated with the presented simulator. Lastly, radar measurements are performed to verify the presented models.

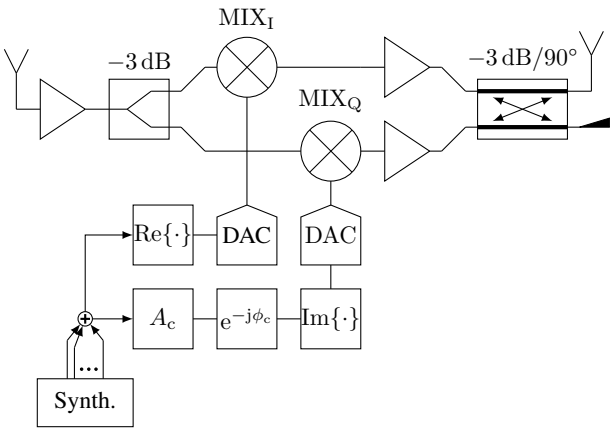

Fig. 1. Block diagram of the modulation-based radar target simulator.

II. System Overview

The basic principle of the RTS is to modulate the radar transmit signal s_TX with a complex sinusoid for each desired target, causing a frequency up- or down shift [5]. In the following we assume that the CS-FMCW radar sends a chirp with an increasing frequency. So a delay in the channel causes a lower frequency of the received chirp compared to the transmitted chirp at the same time instance. Therefore, the RTS has to shift the chirp to a lower frequency in order to simulate a delay. For the simulation of K targets, the radar receive signal s_RX can be expressed as the transmit signal s_TX ideally multiplied by the modulation signal s_mod. The modulation signal consists out of the superposition of K complex sinusoids with individual amplitudes A_k and frequencies $f_{\mathrm{mod},k}$, so

$$\begin{aligned} s_\mathrm{RX}(t) &= s_\mathrm{TX}(t) \cdot s_\mathrm{mod}(t) \\ &= s_\mathrm{TX}(t) \cdot \sum_{k=1}^{K} A_k \exp(-\mathrm{j}2\pi t f_{\mathrm{mod},k})\,. \end{aligned} \tag{1}$$

The design of the modulation-based RTS is depicted in Fig. 1. Since the RTS has to implement a multiplication with complex sinusoids, an inphase quadrature (IQ) mixer is utilized. As a means to reduce costs and circuit complexity, the RTS modulates the radar transmit signal directly, without intermediate frequency (IF) stages. To the knowledge of the authors, no commercially available IQ Mixer suitable for the task of direct modulation exists. Therefore, an IQ mixer capable of direct modulation was realized with two mixers

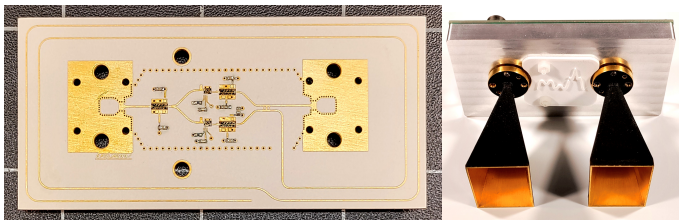

Fig. 2. Printed circuit board (left) and housing with attached horn antennas (right) of the RTS RF-frontend.

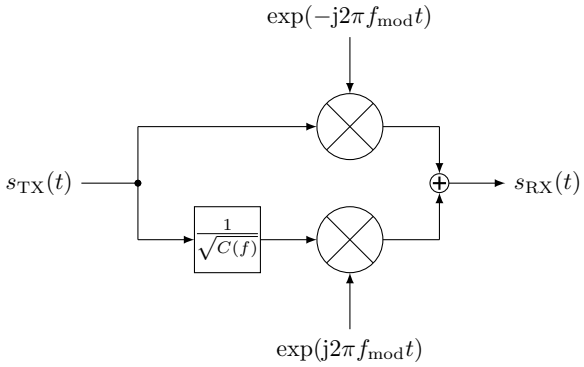

Fig. 3. Block diagram of the model for the sideband suppression $C(f)$.

(UMS CHM2179b98F) and a two-stage branch-line hybrid coupler [9], for the required 90° phase shift between the I- and Q path. Three amplifiers (UMS CHA2080-98F) with a gain of 16 dB are employed to compensate for mixer- and transmission line losses. The amplifiers after the individual mixers act also as buffers since they present impedances with low reflections to the mixers and coupler.

As the automotive CS-FMCW waveform can exhibit bandwidths beyond 1 GHz, the implementation of the IQ mixer must ensure low amplitude- and phase mismatch variations over the allocated frequency band for automotive radars from 76 GHz to 81 GHz [10]. The I- and Q parts of the modulation signal are provided each by a digital-to-analog converter (DAC). Due to the flexibility of generating arbitrary waveforms with DACs, occurring amplitude- and phase mismatches can be compensated digitally. The receive- and transmit antenna are horn antennas that are connected via microstrip-line-to-waveguide transitions. The circuit and its housing with the attached horn antennas is depicted in Fig. 2.

III. Impact of Hardware Nonidealities

Several hardware nonidealities are investigated and their impact on the radar target simulation is derived. For all measurements, the power of the output signal of the RTS is normalized to the RF input signal s_{TX}.

A. Sideband Suppression

The setup with two mixers and a hybrid coupler allows for an ideal single sideband modulation in theory. Because of the frequency dependency of the hybrid coupler's transfer function and due to component variations, only a limited and frequency dependent sideband suppression is realizable. The

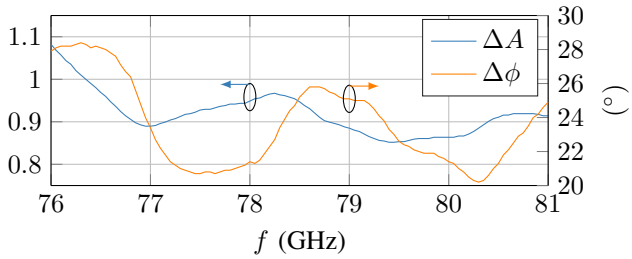

Fig. 4. Measured amplitude- (ΔA) and phase- ($\Delta\phi$) mismatch of the presented RTS.

spectrum of the resulting receive signal $S_{\mathrm{RX}}(f)$ for $f_{\mathrm{mod}} \ll f$ can be modelled as

$$S_{\mathrm{RX}}(f) = S_{\mathrm{TX}}(f) * \delta(f + f_{\mathrm{mod}}) + \frac{S_{\mathrm{TX}}(f)}{\sqrt{C(f)}} * \delta(f - f_{\mathrm{mod}}), \tag{2}$$

where $*$ is the convolution. The second term in (2) corresponds to an additional target, caused by the upper sideband. Therefore, the highest possible sideband suppression $C(f)$ needs to be achieved. The sideband suppression $C(f)$ depends on the amplitude mismatch $\Delta A(f)$—the ratio between the amplitudes—and the phase mismatch $\Delta\phi(f)$—the phase difference error between the I- and Q path. The sideband suppression ratio is calculated as [11]

$$C(f) = \frac{P_{\mathrm{LSB}}}{P_{\mathrm{USB}}} = \frac{\Delta A(f)^2 + 2\Delta A(f)\cos(\Delta\phi(f)) + 1}{\Delta A(f)^2 - 2\Delta A(f)\cos(\Delta\phi(f)) + 1}. \tag{3}$$

The power of the lower and upper sideband is denoted as P_{LSB} and P_{USB}, respectively. So as to maximize the sideband suppression, the compensations for the amplitude mismatch A_{c} and phase mismatch ϕ_{c} are optimized. This means maximizing the energy ratio between the desired target and undesired target for a simplified chirp with a rectangular frequency spectrum as well as an RF frontend with assumed allpass characteristics:

$$\max_{A_{\mathrm{c}},\phi_{\mathrm{c}}} \frac{\int_{f_0}^{f_1} A_{\mathrm{c}}^2\Delta A(f)^2 + 2A_{\mathrm{c}}\Delta A(f)\cos(\Delta\phi(f) - \phi_{\mathrm{c}}) + 1\,\mathrm{d}f}{\int_{f_0}^{f_1} A_{\mathrm{c}}^2\Delta A(f)^2 - 2A_{\mathrm{c}}\Delta A(f)\cos(\Delta\phi(f) + \phi_{\mathrm{c}}) + 1\,\mathrm{d}f}. \tag{4}$$

The integral limits are the lower and upper frequencies of the radar chirp.

In Fig. 4 the phase- and amplitude imbalance of the presented RTS are depicted. Exemplary, for a radar with a chirp bandwidth of 1.8 GHz ranging from 77.2 GHz to 79 GHz, the suppression ratio between the desired target and the undesired target is expected to be −33.4 dB, using the presented RTS.

B. Nonlinearities

Nonlinearities of the circuit components lead to distortions of the signal. The significant devices that have to be considered for the analysis of nonlinearities are the amplifiers and the mixers in the RF path of the system. The mixers are hereby of special interest, since they are inherently nonlinear devices.

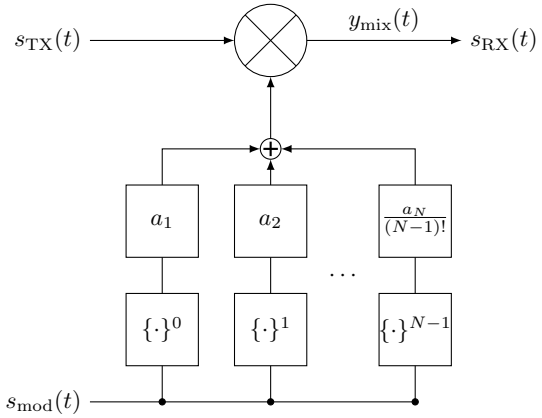

Fig. 5. Block diagram for the significant nonlinearities up to the order N.

The nonlinearities are modelled as memoryless, using a Taylor series. Hence, the output signal $y(t)$ is given by

$$y(t) = \sum_{n=1}^{\infty} \frac{a_n}{n!} x(t)^n \,. \tag{5}$$

For the mixer the quadratic term is the desired one, which realizes the multiplication between the transmit- and modulation signal. At the mixer, the input signal is the sum of the RF-signal and the modulation signal

$$\begin{aligned} x(t) &= s_{\mathrm{TX}}(t) + \sum_{k=1}^{K} A_k \exp(-\mathrm{j}2\pi t f_{\mathrm{mod,k}}) \\ &= s_{\mathrm{TX}}(t) + s_{\mathrm{mod}}(t) \,. \end{aligned} \tag{6}$$

Due to the high frequency of $s_{\mathrm{TX}}(t)$ and the bandpass characteristics of the RTS hardware, only signals containing linear terms of the radar's CW signal $s_{\mathrm{TX}}(t)$ are of significance for the target simulation. Under this assumption, the important products at the mixer output can be reduced by using the binomial theorem to

$$\begin{aligned} y_{\mathrm{mix}}(t) &= \sum_{n=1}^{\infty} \frac{a_n}{n!} \binom{n}{n-1} s_{\mathrm{TX}}(t) s_{\mathrm{mod}}(t)^{n-1} \\ &= s_{\mathrm{TX}}(t) \sum_{n=1}^{\infty} \frac{a_n}{(n-1)!} s_{\mathrm{mod}}(t)^{n-1} \,. \end{aligned} \tag{7}$$

In Fig. 5 the system model for the nonlinearities is outlined. Additional modulation frequencies are generated with

$$m f_{\mathrm{mod},k} \pm q f_{\mathrm{mod},l} \qquad k,l \in \{1,...,K\} \quad m,q \in \mathbb{N}_0 \,. \tag{8}$$

Therefore, the nonlinearity causes additional unwanted targets. The additional targets are simulated at multiples of the intended ranges and velocities due to the harmonics, and combinations of all targets due to the intermodulations. To decrease the power of the intermodulations, the amplitude A_k of the modulation signal has to be retained. This results in significantly higher conversion losses.

The analysis of the amplifiers could be conducted similarly, but the input for of first amplifier in the chain is only the radar transmit signal s_{TX}. This signal is a CW waveform, hence only harmonics are created by the nonlinearity of the amplifier, which can be neglected. The high conversion losses of the mixers, arising from the linearity demands, lead to an input power with a large back-off from the 1 dB compression point of the amplifiers following the mixers. Hence, the mixer dominates the nonlinearities of the entire system, which are depicted in Fig. 6.

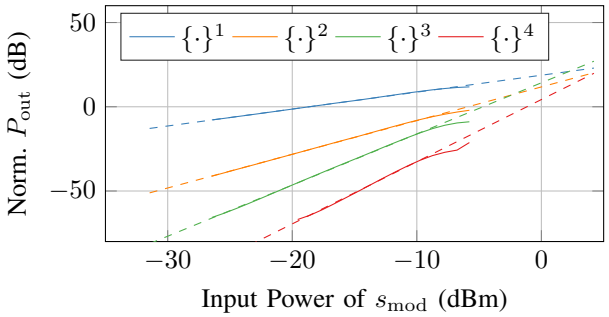

Fig. 6. Power of the RTS's output signal due to the modulation with harmonics of s_{mod}, normalized to the power of s_{TX}.

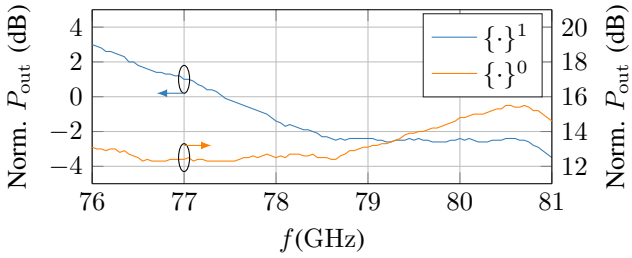

Fig. 7. Power of modulated signal and leaking carrier, normalized to the power of the RF input signal s_{TX}.

C. Carrier Suppression

Another source of undesired targets is the limited carrier suppression. The finite isolation between the mixer's in- and output leads to the RTS relaying the chirp unmodulated back towards the radar. This causes a simulated stationary target at the range of the RTS. This effect can dominate reflections from the simulator's housing. A reduction of the RTS's radar cross section (RCS) by applying absorber or optimizing its shape yields negligible results, since the main reflection is leaking through the circuit. The carrier suppression can be included into the nonlinearity model for $n{=}1$ and its corresponding coefficient a_1 in (7). The limited carrier suppression is especially noteworthy, if the radar itself has a high RCS. Reflections can travel multiple times between radar and RTS, leading to additional undesired targets. The comparison of the modulated and leaking carrier for a modulation signal power of $-18.7\,\mathrm{dBm}$ is shown in Fig. 7.

IV. Measurements

In order to verify the presented models for the hardware limitations, measurements were performed. The measurement setup in an anechoic chamber is depicted in Fig 8. A scenario with two targets (T_1 and T_2) is simulated by the RTS. The

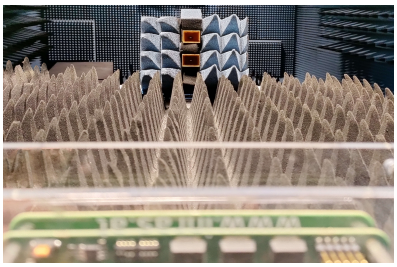

Fig. 8. Photograph of the setup for radar measurements with the RTS.

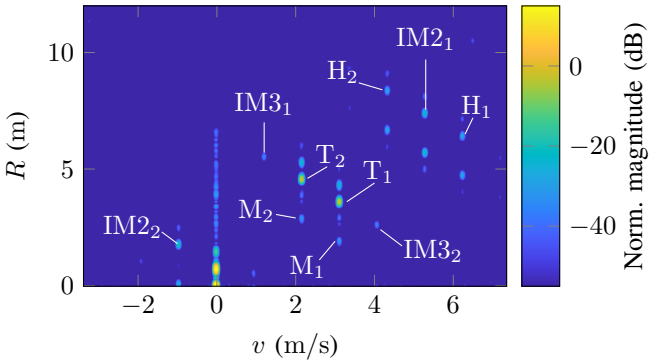

Fig. 9. Magnitude of Rv-plot, normalized to the magnitude of the target T_1.

position and magnitude of the expected additional targets, as a consequence of the hardware nonidealities, are calculated and compared with the measurement data. No absorber was applied to the radar in order to provoke reflections and therefore additional targets due to the carrier leakage. The simulated range of the targets, excluding the time of flight between radar and RTS, is $R_1{=}3\,\mathrm{m}$ and $R_2{=}4\,\mathrm{m}$. The simulated velocity of the targets is $v_1{=}3\,\mathrm{m/s}$ and $v_2{=}2\,\mathrm{m/s}$. Each target is generated by a sinusoid with a power of $-19.4\,\mathrm{dBm}$. In order to reduce variations on account of frequency dependencies of the radar's IF section, it is equalized with the help of a reference measurement. The resulting Rv information with the magnitude normalized to T_1 is outlined in Fig. 9. In Table 1, a comparison between the expected and the measured magnitude in the Rv-processed data is shown. The undesired targets due to the limited sideband suppression are denoted as M_1 and M_2. Targets caused by the quadratic term of s_{mod} are denoted as H_1 and H_2, the intermodulation $\mathrm{IM2}_1$ and $\mathrm{IM2}_2$. Third order intermodulation products of s_{mod} are denoted as $\mathrm{IM3}_1$ and $\mathrm{IM3}_2$. The location and magnitude of the measured target peaks match the expectation based on the models. Solely the power of the mirror frequencies that are caused by nonlinearities cannot be predicted with the here presented models, since the phases of the harmonics generated in the I- and Q branch of the RTS do not fulfill the required phase difference for single sideband modulation. The reflections at the radar that are amplified by the carrier leakage of the RTS manifest themselves as undesired targets with a $0.7\,\mathrm{m}$ offset from all predicted targets. The magnitude of those targets is not predictable, since the RCS of the radar is unknown beforehand.

Table 1. Comparison between expected and measured performance

Name	Location (v, R)	Expected	Measured
T_1	$(v_1, R_1{+}R_{\mathrm{RTS}})$	0 dB	0 dB
T_2	$(v_2, R_2{+}R_{\mathrm{RTS}})$	0 dB	−0.2 dB
M_1	$(v_1, R_1{-}2R_{\mathrm{RTS}})$	−33.4 dB	−30.6 dB
M_2	$(v_2, R_2{-}2R_{\mathrm{RTS}})$	−33.4 dB	−30.4 dB
H_1	$(2v_1, 2R_1{+}R_{\mathrm{RTS}})$	−25.9 dB	−26.5 dB
H_2	$(2v_2, 2R_2{+}R_{\mathrm{RTS}})$	−25.9 dB	−26.5 dB
$\mathrm{IM2}_1$	$(v_1{+}v_2, R_1{+}R_2{+}R_{\mathrm{RTS}})$	−19.9 dB	−19.9 dB
$\mathrm{IM2}_2$	$(v_2{-}v_1, R_2{-}R_1{+}R_{\mathrm{RTS}})$	−19.9 dB	−19.3 dB
$\mathrm{IM3}_1$	$(2v_1{-}v_2, 2R_1{-}R_2{+}R_{\mathrm{RTS}})$	−34.5 dB	−34.9 dB
$\mathrm{IM3}_2$	$(2v_2{-}v_1, 2R_2{-}R_1{+}R_{\mathrm{RTS}})$	−34.5 dB	−35.3 dB

V. Conclusion

In this paper, the hardware setup of a new RTS for automotive CS-FMCW radars is presented. The direct modulation principle allows for a compact RF-frontend and low hardware complexity. Besides, models for occurring hardware nonidealities are derived and their influence on the target simulation is discussed. The models are successfully verified with radar measurements by comparing the expected and measured additional target responses that stem from hardware nonidealities of the RTS.

Acknowledgment

This work was supported by the German Federal Ministry of Education and Research through the project SecForCARs under grant 16KIS0797.

References

[1] S. Lutz, C. Erhart, T. Walter, and R. Weigel, "Target simulator concept for chirp modulated 77 GHz automotive radar sensors," in *11th Eur. Radar Conf.*, 2014, pp. 65–68.

[2] M. Engelhardt, F. Pfeiffer, and E. Biebl, "A high bandwidth radar target simulator for automotive radar sensors," in *Eur. Radar Conf. (EuRAD)*, 2016, pp. 245–248.

[3] J. Sobotka and J. Novak, "Digital vehicle radar sensor target simulation," in *IEEE Int. Instrum. and Meas. Technol. Conf. (I2MTC)*, 2020, pp. 1–5.

[4] T. Dallmann, J. Mende, and S. Wald, "Atrium: A radar target simulator for complex traffic scenarios," in *IEEE MTT-S Int. Conf. on Microw. for Intell. Mobility (ICMIM)*, 2018, pp. 1–4.

[5] J. Iberle, P. Rippl, and T. Walter, "A near-range radar target simulator for automotive radar generating targets of vulnerable road users," *IEEE Microw. and Wireless Compon. Lett.*, vol. 30, no. 12, pp. 1213–1216, 2020.

[6] C. Waldschmidt, J. Hasch, and W. Menzel, "Automotive radar — from first efforts to future systems," *IEEE J. Microwaves*, vol. 1, no. 1, pp. 135–148, Jan. 2021.

[7] J. Hasch, E. Topak, R. Schnabel, T. Zwick, R. Weigel, and C. Waldschmidt, "Millimeter-wave technology for automotive radar sensors in the 77 GHz frequency band," *IEEE Trans. on Microw. Theory and Techn.*, vol. 60, no. 3, pp. 845–860, 2012.

[8] P. Schoeder, V. Janoudi, B. Meinecke, D. Werbunat, and C. Waldschmidt, "Flexible direction-of-arrival simulation for automotive radar target simulators," *IEEE J. Microwaves*, vol. 1, no. 4, pp. 930–940, Oct. 2021.

[9] R. Levy and L. Lind, "Synthesis of symmetrical branch-guide directional couplers," *IEEE Trans. on Microw. Theory and Techn.*, vol. 16, no. 2, pp. 80–89, 1968.

[10] FCC, "Radar services in the 76-81 GHz band," https://docs.fcc.gov/public/attachments/DOC-345476A1.pdf, 2017.

[11] S. A. Maas, *Microwave Mixers*. Artech House, 1986.